



Review

A Review on Wire-Fed Directed Energy Deposition Based Metal Additive Manufacturing

Tuğrul Özel ^{1,*}, Hamed Shokri ²  and Raphaël Loizeau ^{1,3}

¹ Manufacturing and Automation Research Laboratory, Department of Industrial and Systems Engineering, Rutgers University-New Brunswick, Piscataway, NJ 08854, USA

² Chair of Materials Science and Additive Manufacturing, Mechanical Engineering and Safety Engineering, Bergische Universität Wuppertal, 42119 Wuppertal, Germany

³ Faculty of Science and Engineering, Chemistry Department, Materials Engineering for Aeronautics and Space, Université Toulouse III-Paul Sabatier, 31062 Toulouse, France

* Correspondence: ozel@rutgers.edu; Tel.: +1-848-445-1099

Abstract: Metal additive manufacturing has reached a level where products and components can be directly fabricated for applications requiring small batches and customized designs, from tinny body implants to long pedestrian bridges over rivers. Wire-fed directed energy deposition based additive manufacturing enables fabricating large parts in a cost-effective way. However, achieving reliable mechanical properties, desired structural integrity, and homogeneity in microstructure and grain size is challenging due to layerwise-built characteristics. Manufacturing processes, alloy composition, process variables, and post-processing of the fabricated part strongly affect the resultant microstructure and, as a consequence, component serviceability. This paper reviews the advances in wire-fed directed energy deposition, specifically wire arc metal additive processes, and the recent efforts in grain tailoring during the process for the desired size and shape. The paper also addresses modeling methods that can improve the qualification of fabricated parts by modifying the microstructure and avoid repetitive trials and material waste.

Keywords: directed energy deposition; wire; grain; microstructure; metals; 3D printing; additive manufacturing



Citation: Özel, T.; Shokri, H.; Loizeau, R. A Review on Wire-Fed Directed Energy Deposition Based Metal Additive Manufacturing. *J. Manuf. Mater. Process.* **2023**, *7*, 45. <https://doi.org/10.3390/jmmp7010045>

Academic Editors: Geoffrey R. Mitchell and Mohamed A. Elbestawi

Received: 14 December 2022

Revised: 23 January 2023

Accepted: 30 January 2023

Published: 8 February 2023



Copyright: © 2023 by the authors. Licensee MDPI, Basel, Switzerland. This article is an open access article distributed under the terms and conditions of the Creative Commons Attribution (CC BY) license (<https://creativecommons.org/licenses/by/4.0/>).

1. Introduction

Continued interest in additive manufacturing (AM) has grown over the last decade to the point where the trend in industry is to adopt this technology to overcome the drawbacks (manufacturing time, cost, supply) of conventional manufacturing. Due to the feasibility of the economical production of large-scale metal components with quite high deposition rates [1,2], a remarkable improvement has been achieved in the perception of metal additive manufacturing (AM) processes and in the microstructure and mechanical properties of built parts. Most additively manufactured metal parts suffer from weaker mechanical and physical properties resulting from columnar grain structure.

Among the seven general classes of additive manufacturing, two are mainly used for metallic aerospace applications: directed energy deposition (DED) and powder bed fusion (PBF) [3,4]. In PBF, the stock material is fused locally in a powder bed by using either a moving laser beam (LPBF) or coil-controlled electron beam (EBPBF), which creates a melt pool that transfers the powder into liquid metal then solidifies when the locality cools off during layerwise processing. In DED, the material is locally deposited using feeding wire or powder feedstock right into the melt pool. The melt pool is made by lasers, electron beams, electrical arc, plasma, or any other energy source (see Figure 1). DED AM processes that use laser beam heat energy include laser wire DED (LW-DED) or laser powder DED (LP-DED). Other heat energy sources, such as electron beam, plasma,

and electric arc, are used in wire electron beam DED (EB-DED), plasma wire DED (PW-DED), and wire arc DED (WA-DED), also known as wire arc AM (WAAM), respectively. Lastly, kinetic energy deposition based powder cold spray is a promising technology worth mentioning. Each class of DED processes has its pros and cons due to component size, geometry, manufacturing speed, and surface properties, which make the process more suitable for a specific application. Sensitivity analysis and modeling results show that in comparison to other metal AM methods, wire arc DED AM has remarkable potential as an efficient approach in manufacturing. Sensitivity analysis generally identifies indirect costs as a key cost driver, with parts per build plate and shielding cost having significance for smaller and larger parts, respectively [5]. Recently, an alternative approach was introduced by Dugar et al. [6] in the fabrication of Al-Si5 alloy using a robotic MIG-based instrument. The system consists of a CAD/CAM plus combined WAAM hybrid process that achieves sustainably high productivity via structural alloys.

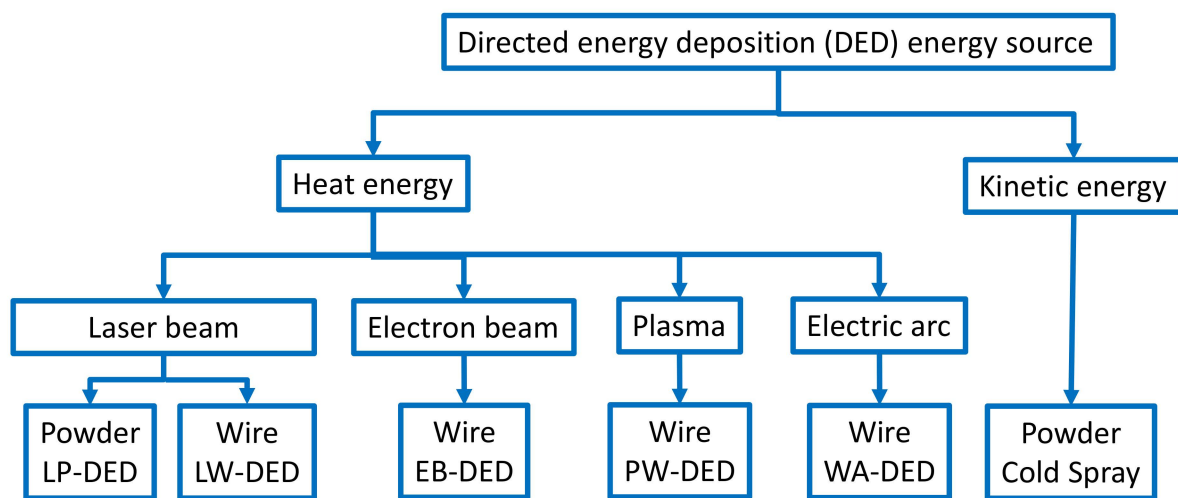


Figure 1. Categories of directed energy deposition in terms of energy source and feedstock.

In metal wire-fed DED AM, the relationship between microstructure and material composition governs the fabrication quality and properties of the material [7]. Due to the thermal process, predicting and controlling the microstructural evolution is challenging in this technique. AM processes typically lead to columnar grain structures that are prejudicial to mechanical properties [8,9]. However, very fine equiaxed grains can be obtained by choosing alloys with enough solute to generate a sufficient cellular structure (CS). Furthermore, a large amount of thermal undercooling can be generated by the very high cooling rates, and this can facilitate nucleation. Mechanical means of grain refinement such as ultrasound oscillations or interpass cold rolling can also be effective [7]. Further research studies are being pursued on other approaches in order to refine grains and optimize the AM process to improve mechanical properties. Process stability improvement, decreasing or eliminating defects of deposition, and fabricating components with high mechanical performance and quality have become the main focuses of research on making the wire-fed DED manufacturing process more competitive against other AM methods. Wire-fed DED systems are an interdisciplinary challenge for metal components and are expected to be developed and optimized for a certain application, rather than a single system that is capable of addressing all of the possible problems. In terms of popular AM applications, AM-fabricated titanium alloys have been used in various industries as an alternative to conventional routes [8]. High corrosion resistance, low weight-to-strength ratio, and high-temperature resistance properties make titanium alloys prime candidates for use in aerospace industries. High thermal resistance, ductility, and strength are the other promising properties of titanium alloys and also make it very difficult to process with machining. In addition, machining, like subtractive manufacturing, is inefficient in terms

of time spent on material removal and chips produced as material waste. Recently, wire-fed additive manufacturing has received increasing attention from aerospace industries due to its ability to directly fabricate large-scale metal components [7]. To significantly reduce the machining and consequently the process cost after the fabrication of the components, near-net-shape (NNS) manufacturing shows an alternative path [10]. Hybrid manufacturing is the integration of additive manufacturing methods with a machine that is in charge of subtractive processes. To overcome the shortcoming of decreasing the ability of the components after manufacturing, besides the desired strength and hardness, hybrid manufacturing is introduced and implemented [11,12].

Nowadays, wire-fed DED AM is a promising process for the fabrication of metal components such as nickel alloys [13–15], aluminum, steel [16,17], and chiefly titanium. Wire-fed DED AM, in particular WAAM, can result in fabrication and post-processing time reduction in comparison with traditional processes. For instance, WAAM technology enabled nearly 90% of raw material saving in a Ti6-Al4-V external landing gear assembly [8]. WAAM is a novel method that allows for the bulk production of large components with greater production rates (several kg/h) [9,18]. The unit wire material cost is nearly half of the powder material for all three alloys presented, depicting the cost advantage of wire DED AM processes. A comparison of wire and powder feedstock commercial markets is given for wire DED AM and PBF-AM in Table 1. However, the thermal gradient and the high cooling rates of the fusion-based metal AM process often lead to an almost exclusively columnar grain microstructure (especially in titanium-based alloys), which can result in anisotropic mechanical properties that are, as a consequence, undesirable [9,19].

Table 1. Material feedstock commercial market (2022) comparison for a few metal alloys.

Material Feedstock	Titanium Ti-6Al4V	Tantalum	Inconel 625
Wire (0.9 mm diameter)	~USD120/kg	~USD1100/kg	~USD55/kg
Wire (1.1 mm diameter)	~USD110/kg	~USD1100/kg	~USD55/kg
Wire (1.6 mm diameter)	~USD100/kg	~USD1000/kg	~USD55/kg
Wire (2.4 mm diameter)	~USD97/kg	~USD950/kg	~USD50/kg
Wire (3.2 mm diameter)	~USD95/kg	~USD900/kg	~USD50/kg
Wire (4.0 mm diameter)	~USD92/kg	~USD900/kg	N/A
Powder AM grade	~USD250/kg	~USD1100/kg	~USD100/kg

Producing a component with the additive manufacturing concept has existed for decades. AM is defined as the process of incrementally creating matter from computer model data, layer by layer, in order to create a three-dimensional functional object [20]. In recent years, AM has begun to emerge as a viable new manufacturing process for metallic aerospace components [8,21]. AM processes are progressively becoming more accepted and deployed in regard to certified aerospace applications. One of the major reasons for this is the significant waste and cost reduction, and it allows direct and quick production for the replacement of obsolete parts [22]. Studies have shown that the aerospace industry acknowledges a constant growth for AM for aircraft components, which in 2017 represented 18.8% of the global industry market share instead of 16.6% in 2016 [20–23]. Many AM technologies are available, and ample progress is being made every day in testing and research on metal AM processes. It is essential to understand these technologies to choose the one that will fit the best into the application at hand. The manufacturing process is chosen according to the components manufactured. Indeed, mechanical properties (strength, durability, stiffness, toughness, etc.) depend on microstructure, which is mainly determined by the process parameters [1,3].

According to the ASTM F42 Committee on additive manufacturing, there are seven standard categories and four related to metal AM, including DED and PBF [23]. This review paper focuses on wire-fed DED processes, in particular wire arc additive manufacturing

technology. DED is defined by ASTM F2792 as “an additive manufacturing process in which focused thermal energy is used to fuse materials by melting as they are being deposited”. The heat source can be a laser (Figure 2a,b), electron beam (Figure 2c), or electric arc (Figure 2d) (or plasma arc, tungsten-inert gas, or metal-inert gas arc), whereas the feedstock can be metal powder or wire.

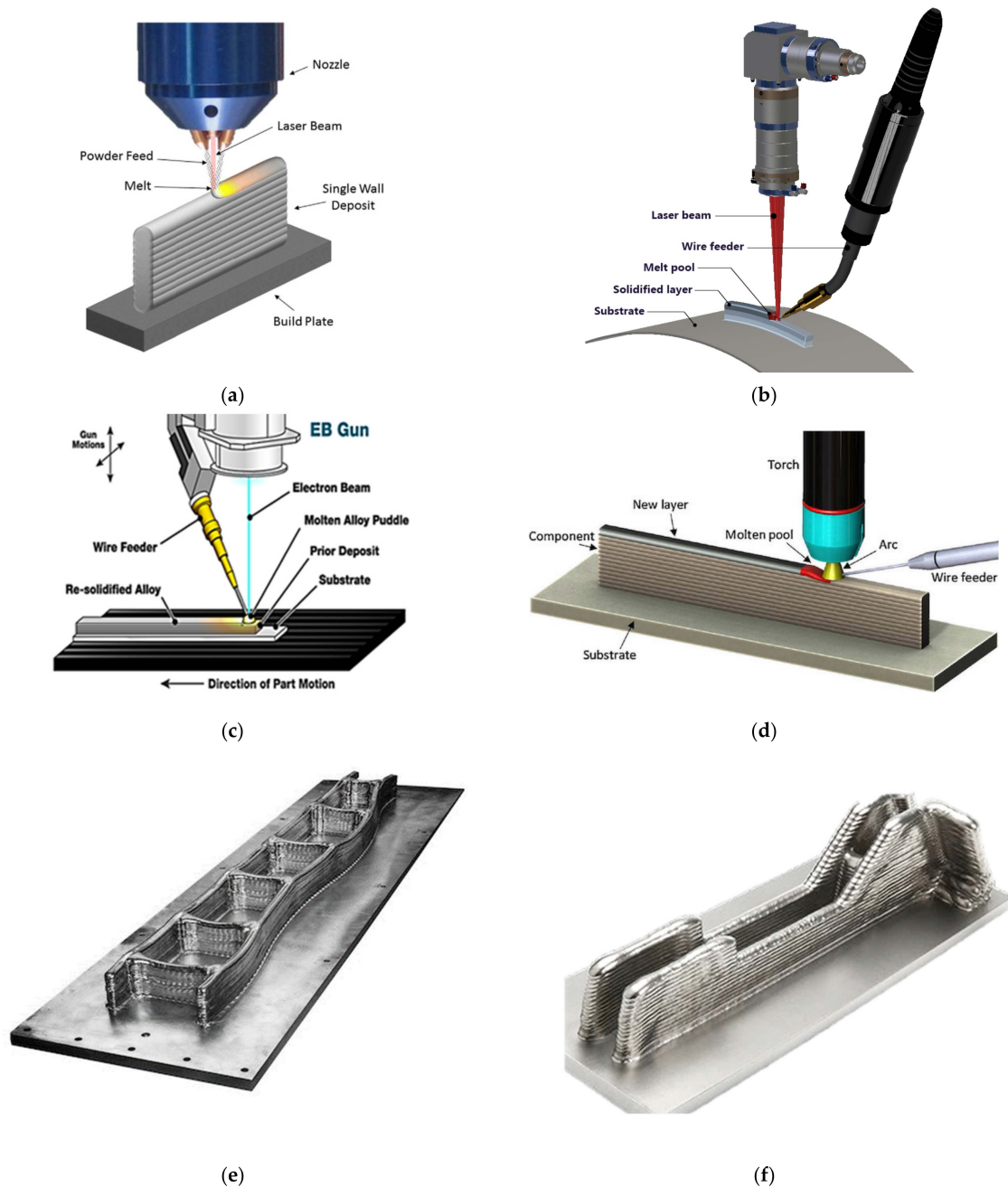


Figure 2. (a) Laser, powder-fed DED (LP-DED) system [24]; (b) laser, wire-fed DED (LW-DED) system [25], (c) electron beam, wire-fed DED (EB-DED) system [26]; (d) electric arc, wire-fed DED (WA-DED) system [27]; (e) WA-DED model of a 3.94-foot (1.2 m) Ti6Al4V wing spar [10]; and (f) PW-DED aircraft structural component from Ti6Al4V using Norsk Titanium’s rapid plasma Deposition process [10]. Images in (a), (b), (c), (d) are reproduced with permission from authors in [24–27] respectively. Images in (b), (c), (e) and (f) are reproduced with permissions from Procada, Sciaky, Welding and Additive Manufacturing Centre, Cranfield University, and Norsk Titanium respectively.

Although laser powder bed fusion (LPBF) is mainly used for small- to medium-sized components with complex geometries, laser-based DED (also known as laser-engineered net shaping (LENS) or laser metal deposition (LMD)) is based on a material feed system that places the wire or powder onto the point to be melted by laser energy (at the interaction spot between feedstock and laser). This method of 3D printing is more suitable for large components along with high building rate speeds when compared to conventional LPBF systems. Most systems use a nozzle mounted on a multi-axis arm that can move in multiple directions. The substrate can be in a three-axis system (stationary position) or in a rotating five-axis system. This increases the ability of the machine to process more complex geometries [23]. DED for metal AM requires post-processing to obtain good surface and mechanical properties. Surface texture is explored by Özel et al. [28] using image processing together with machine-learning-based algorithms. A thermal process is used to improve mechanical properties by reducing residual stresses, and to achieve the desired final geometry, parts produced using DED are usually near-net shapes. A build chamber provides laser safety, and the chamber may be filled with inert gas to prevent the fused material from oxidation. For more reactive metals, such as titanium, the chamber is flooded with argon or nitrogen, since even a small amount of oxygen can result in an undesirable reaction, but for nonreactive metals, a gas directed at the melt pool may provide enough resistance to oxidation. Moreover, a vacuum pump may be used to reduce the oxygen content and create a crossflow for plume removal. DED processes are characterized according to the heat source and the feedstock. This research focuses on technology using arc electricity as heat source and wire as feedstock, hence the WAAM process.

In recent years, interest from the industrial sector in WAAM has been growing due to its capability of producing large metallic components with a high deposition rate [1,2] and the potential for notable cost and material savings [27]. As shown in Figure 2b–d, using wire as feedstock provides an important cost reduction compared to powder. Moreover, research studies show that energy consumption and material waste are comparatively lower than the laser or electron beam process using wire as feedstock [28]. The utilization of an electric arc as heat source induces nonuniform thermal expansion and stress during deposition, leading to a heterogeneous microstructure and therefore anisotropic properties for the produced parts. First, a description of the WAAM processes will be given for understanding the advantages and defects of these processes. Then, the material available for this process will be briefly presented. There are mainly three types of WAAM processes: (i) gas melting arc welding (GMAW)-based, (ii) plasma arc welding (PAW)-based, and (iii) gas tungsten arc welding (GTAW)-based [29]. The choice of technique induces the process parameters and the production rate of the component. Within these processes, there are essentially two WAAM systems that differ according to their chamber. One has a good inert gas shielding environment provided by an enclosed chamber. The second system uses designed local gas shielding mechanisms. This last system is more suitable to fabricate huge metal components even to several meters in dimension. There are three main steps involved in compound fabrication: planning of the process, deposition, and post-processing. For the deposition process, programming software is used to control the welding parameters (speed, intensity) and robot motions. During deposition, advanced WAAM systems can be equipped with various sensors to measure metal transfer behavior, deposited surface geometry, interpass temperature, and welding signals, to attain the product in high quality. This is an area of current research with the aim of significantly improving WAAM process performance. For example, recently, interpass cooling has been developed to obtain the desired mechanical properties and microstructure and may reduce residual stress and distortion. WAAM processes use wires of alloys as feedstock material in a wide range. Titanium alloys have been widely studied for AM in aerospace components due to their high material cost and high strength-to-weight ratio. The WAAM process is an alternative to produce more efficient components at a lower cost than the conventional subtractive manufacturing methods, especially for large-sized titanium components with complex structures [26].

Aluminum alloys with many different series, Al-Si (4xxx), Al-Mg (5xxx), and some series of Al-Cu (2xxx) have been successfully used for large and complex structures to justify the WAAM process, since the cost of manufacturing small and simple aluminum alloy component using conventional machining is low. For the same reason, using WAAM to fabricate steel is not very popular because it is the most commonly used engineering material. WAAM is not used for some series, such as Al (7xxx), Al (6xxx), and most types of Al-Cu (2xxx), which are challenging to weld due to a turbulent melt pool, weld defects, and hot cracking possibility because of Cu content, which occur during the deposition process.

After titanium alloys, nickel-based superalloys are also one of the most popular materials studied by the AM research community because of their high strengths at elevated temperatures and high production cost using traditional methods. Most research is on Inconel 718 and Inconel 625, which are very interesting alloys for the aeronautical, aerospace, chemical, petrochemical, and marine industries due to their outstanding strength and oxidation and resistance at temperatures over 550 °C. AM parts show anisotropic properties with columnar grains between layers. Columnar grains grow perpendicular to the solidification surface, and their crystalline orientation is in the grain growth direction.

It is well known that thermal history during the fabrication process affects the microstructure of the product. Inhomogeneous composition and meta-stable microstructures are the consequences of the thermal cycle during the WAAM process (heating and cooling) in the fabricated component. For example, anisotropic properties with higher elongation values and lower strength have been observed in the build direction (Z) compared to deposition direction (X) in WAAM-fabricated Ti-6Al-4V samples, which are mainly attributed to the orientation of the elongated prior β grains and the grain size of α lamellae [30].

2. Grain Size and Morphology

A lot of research has been pursued to better understand the relationships that exist between composition–processing–microstructure for materials produced by additive manufacturing [31,32]. These research studies are usually based on the interdependence model. The following section will first define what the interdependence model is before developing some research that leads to grain refinement in titanium alloys.

Research has shown that AM such as PBF or DED for metals produces textured grain structures (columnar grains) in most metals, such as titanium [33–38], stainless steel [2,39–43], and aluminum alloys [1]. Columnar grains are usually unwanted, as their presence can lead to solidification defects and mechanical property anisotropy. However, columnar grains are difficult to avoid in AM metal parts. This can be explained by the nature of AM, which involves small-scale localized solidification that occurs under significant thermal gradients (G) with high cooling rates (T), which favor dendritic–columnar structures during solidification (see Figure 3). The columnar grain morphology is also accentuated because in AM, each successive layer grows epitaxially from the last, and there is, therefore, no barrier to nucleation [44]. Each new layer implies partially melting back the previous layer to help prevent a lack of fusion defects [45]. Thus, equiaxed grains that may form in the final layer (lower G and T) are susceptible to remelting and resolidifying as columnar grains when the next layer is deposited. A solution to the issue of large directional grains is to introduce either a solute that promotes constitutional supercooling or to add potent nuclei or a combination of the two. The interdependence model shows the interdependence between particle potency, solute, and process parameters in creating an equiaxed structure.

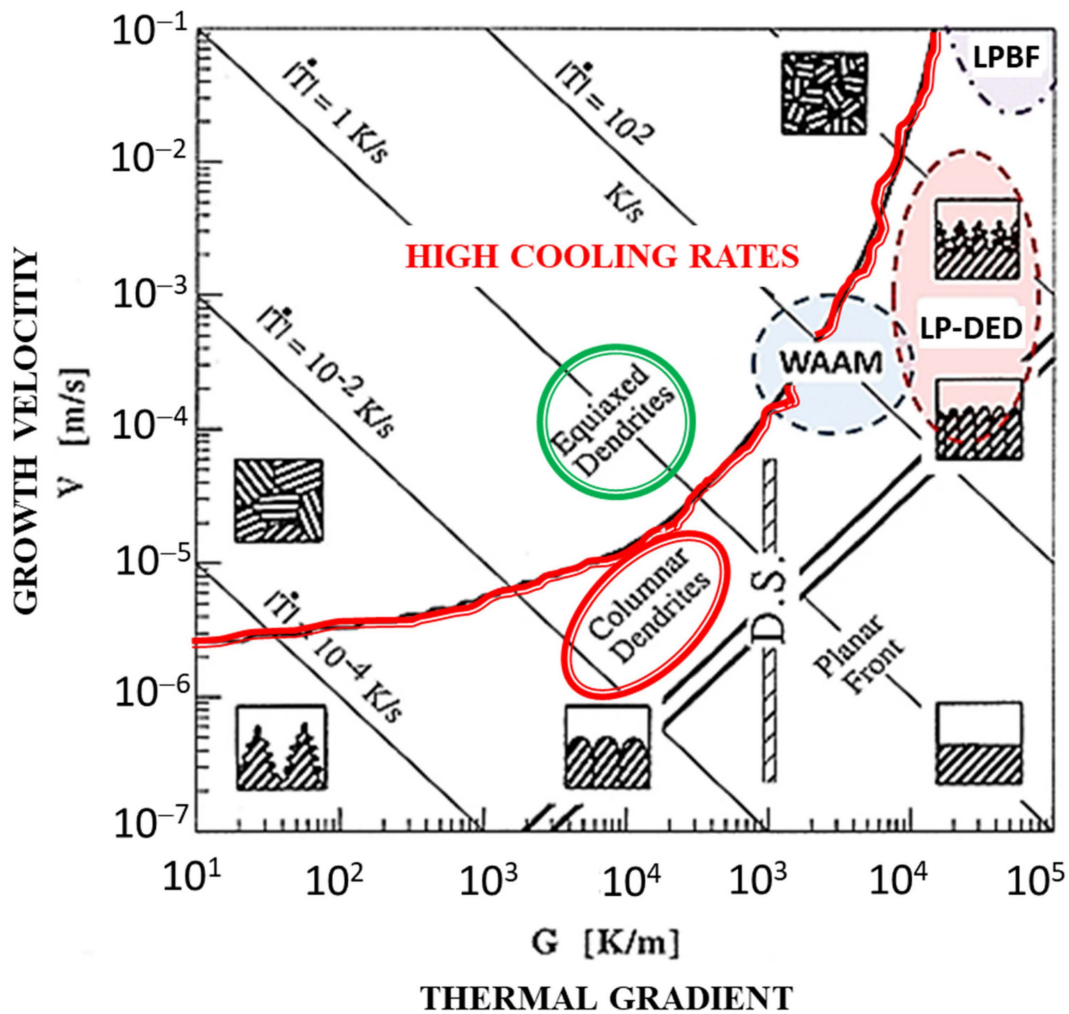


Figure 3. Small melt pools, high cooling rates (T), growth velocities (v), and thermal gradients (G) during the majority of AM processes favor the formation of columnar dendrites. The figure is adopted with permission from authors in [46].

According to the interdependence model, the final grain size is determined by three components: (i) the distance from this S/L interface to the point where this critical amount of constitutional supercooling has been generated (x'_{dl}); (ii) the additional distance to the nearest most potent nucleant particle; and (iii) the distance that a previously nucleated grain must grow in order to establish sufficient constitutional supercooling ahead of a solid–liquid interface to enable the nucleation of the next grain (x_{cs}) [47]. Therefore, there is a zone (sum of x_{cs} and x'_{dl}) where nucleation is completely suppressed. This is called the nucleation-free zone (NFZ). To promote nucleation and improve grain refinement, it is critical to minimize the nucleation-free zone. Table 2 summarizes the key parameters that can be manipulated to increase the likelihood of nucleating equiaxed grains [44].

Table 2. Key alloy and solidification parameters that enhance nucleation. The data is reproduced with permission from authors in [44,46].

Factors That Minimize the Size of the Nucleation-Free Zone	Factors That Minimize x_{sd}
Minimize D : this will encourage a narrow solute pile up and faster generation of ΔT_{CS}	Increase the particle density: more particles per volume of melt increases the probability of their presence at the end of the nucleation-free zone
Minimize ΔT_n : this will allow nucleation sooner (less ΔT_{CS} is required)	Increase the potency of the particles: a low ΔT_n will require less thermal or constitutional supercooling
Minimize z : the newly nucleated equiaxed grain will not need to grow as much and instead requires only an incremental contribution to ‘top up’ the net ΔT_{CS} . z is a product of the temperature gradient G and is small when G is small	Particle size has also been associated with potency
Maximize Q : solutes with high Q will rapidly develop ΔT_{CS}	Create a homogeneous size and spatial distribution of particles within the melt
Maximize V : this will encourage a narrow solute pile up and ΔT_{CS}	Maximize chemical stability of the particles in the liquid metal

According to this model, the following equation provides very good predictions of grain size, close to the experimentally measured grain size obtained in Equation (1). A small grain size results from small values of D and ΔT_n and large values of v and Q . From an experimental point of view, reducing the value of ΔT_n means using larger particles, which could be deleterious to post-processing and mechanical properties. Therefore, increasing v means changing the process parameters, and increasing Q is possible by changing the alloy composition, which could be more effective to reduce grain size. Thus, research studies in grain refinement are usually based on the interdependence model because it is able to illustrate mechanisms of grain refinement and provide directions to improve the ability to accurately predict the grain size of alloys made by additive manufacturing.

$$d_{gs} = \frac{1}{\sqrt[3]{\rho f}} + \frac{D\Delta T_n}{vQ} \tag{1}$$

- d_{gs} : grain size (μm);
- ΔT_n : undercooling for nucleation ($^\circ\text{C}$);
- D : diffusion rate in the liquid ($\text{m}^2 \cdot \text{s}^{-1}$);
- v : growth of the solid–liquid interface velocity ($\text{m} \cdot \text{s}^{-1}$);
- Q : growth restriction factor ($Q = C_0 m (k - 1)$);
- C_0 : alloy composition (%wt);
- m : slope of the liquidus;
- k : solute partition coefficient;
- ρ : inoculant particle density added to the melt;
- f : particle fraction that successfully nucleates a grain.

3. Process Parameters

To promote the columnar-to-equiaxed transition (CET), one approach is to manipulate the processing parameters during AM to affect the growth rate of the S/L interface (v), the temperature gradient (G), and the cooling rate (T) (induced by G and v) [34]. Some studies have investigated the optimum process parameters and their effects on the microstructure, hardness, and mechanical properties in WAAM [48], and some others have shown that the CET occurs when G decreases and v increases. Based on the work of Bontha et al. [49], who

modeled the condition of the solidification for Ti-6Al-4V laser AM, Xu et al. [50] reported the equiaxed grain presence in Ti-6Al-4V selective laser melting (SLM) after manipulating the process parameters to reduce G (by increasing the laser power). The drawback is the large equiaxed grains formed under high laser power during Ti-6Al-4V deposition. Therefore, processes that promote CET are usually coupled with grain-refining processes. Erdakov et al. [51] observed the impact of the deposition track of Ti-6Al-4V powders on the microstructure in the SLM process. They demonstrated a basket weaving structure consisting of α and β phases, which is a mechanical texture. Kushwaha et al. [52] also investigated the effect of process parameters (scanning strategy and speed, hatch spacing, layer thickness, and laser power) on the mechanical properties, density, and microstructure of Ti-6Al-4V parts fabricated with SLM. Zhang et al. [53] observed equiaxed grains at lower energy densities and columnar grains at higher laser energy densities during Ti-6Al-2Sn-2Zr-3Mo-1.5Cr-2Nb laser metal deposition. This might seem, at first glance, in contradiction with the predictions made by Bontha et al. [49] (which expect CET at higher laser density). However, in this model, the effect of changing nucleation factors (nucleation undercooling ΔT_N , nucleation population, etc.) or powder deposition rate was not included in the calculation. Therefore, Zhang et al. proved that the tendency for the CET increased with increasing the powder deposition rate by providing heterogeneous nucleation on partially unmelted powder particles [34]. On the other hand, it was observed that when the laser energy density increased, the survival rate of unmelted particles reduced, and therefore it reduced the nucleation rate.

To improve deposition rate and reduce porosity [2], hot-wire arc additive manufacturing (HWAAM) has been applied as a new method by several research groups [1,38,54,55]. The HWAAM principle is that when the wire is connected to the parts or the substrate, resistance heat is generated, and it is utilized to reduce arc energy input and improve wire surface conditions.

Ti-6Al-4V alloy components were fabricated using WAAM by Wang et al. [56], and the presence of equiaxed and columnar grain zones was investigated. Equiaxed grains at the bottom and the columnar grains on them were shown. It is indicated that changing deposition parameters such as welding current could affect the volume fraction of the equiaxed grain zone.

Combined processes in WAAM titanium alloy were studied by Zhuo et al. [57], aiming at columnar β grain refinement. The combination of an ultra-high pulse frequency arc, adding boron particles, and ultrasonic vibration was used to examine their impact on grain morphology and α texture. The results of the low-frequency pulse arc and the boron particles were promising in grain refinement.

The effect of rolling deformation on recrystallization and subsequently grain refinement in a WAAM process of Ti alloy was investigated by Davis et al. [58]. A radiused roller was used for the deformation of the added layer surface after each deposition.

The effect of the solidification temperature gradient on the structure and morphology of the Ti-6Al-4V WAAM process was investigated by Hönnige [59]. It is demonstrated that grain refinement and equiaxed structure are observed at lower-temperature gradients and mainly in the top last layer.

Rolling sequentially during the WAAM process of Ti alloy was represented as an effective path to refine the β grains by Donoghue et al. [60]. Less than 20% reduction was applied after each layer deposition, and it was proposed to increase the deformation for more refinement.

McAndrew et al. [27] and Ding et al. [61] used interpass rolling in a WAAM process of titanium alloy components as a grain refinement method. Various process parameters, such as roller type, applied force, and roller diameter, were investigated. The results demonstrated significant refinement by increasing the force and roller size. Homogeneity during the refinement depended on the fabricated component features and the roller design.

Brandl et al. [62] investigated the morphology, microstructure, chemical composition, and hardness of additively manufactured Ti-6Al-4V blocks. Ti-6Al-4V blocks were

fabricated using a wire-fed system processed with a Nd/Yag laser. Various process parameters and post-heat treatments were studied. They found that post-heat treatment above 995 °C could change size and morphology and also hardness but does not necessarily lead to grain refinement. However, exposure to 1200 °C can cause a change in morphology totally. Prior columnar grains were replaced by equiaxed grain colonies, and it seemed to be due to recrystallization under high temperature. Artaza et al. [63] studied the impact of different heat treatment atmospheres on the properties of Ti-6Al-4V walls manufactured by the WAAM-PAW method. They also compared the obtained properties with a thermomechanical simulation to find out the effect of different media (vacuum, air, and argon).

The interpass rolling impact in a Ti-6Al-4V WAAM process on β grain size was investigated by Martina et al. [64]. Consequently, the transition of the columnar structure to equiaxed was shown due to interlayer rolling.

4. Alloy Composition

Although G and v are significant parameters influencing the CET, the alloy constitution (which favors nucleation) is also important to achieve equiaxed grain morphology. For the CET to happen, it is necessary for a supercooling zone to exist ahead of the columnar front for a significant amount of grain to nucleate and for detached solid fragments of unmelted powders to survive and grow. Multiple research studies have shown that alloy solute plays a significant role in generating constitutional supercooling (ΔT_{CS}). The rate at which a solute generates constitutional supercooling is determined by the growth restriction factor, Q . Solutes with important Q values rapidly generate ΔT_{CS} and are considered as growth-restricting solutes that can provide effective grain refinement [34]. The Al and V solute in Ti-6Al-4V provides no ΔT_{CS} (they have negligible Q values in Ti [65]), whereas Cr and C can provide ΔT_{CS} in Ti. Thus, CET is hard to achieve in Ti-6Al-4V during AM. Wang et al. [66] demonstrated this point when fabricating a compositionally graded Ti-6Al-4V to Ti-25V-15Cr-2Al-0.2C component by laser metal deposition using a combined Ti-6Al-4V wire feed source and Ti-25V-15Cr-2Al-0.2C powder. Initially, the 100% Ti-6Al-4V part of the component generates columnar grains but equiaxed grains resulted as soon as composition grading began, resulting in the Ti-6Al-4V alloying with Cr and C. Bermingham et al. [34], studied the composition and thermal sensitive factors affecting the CET during wire-based additive manufacturing of titanium alloys (see Figure 4).

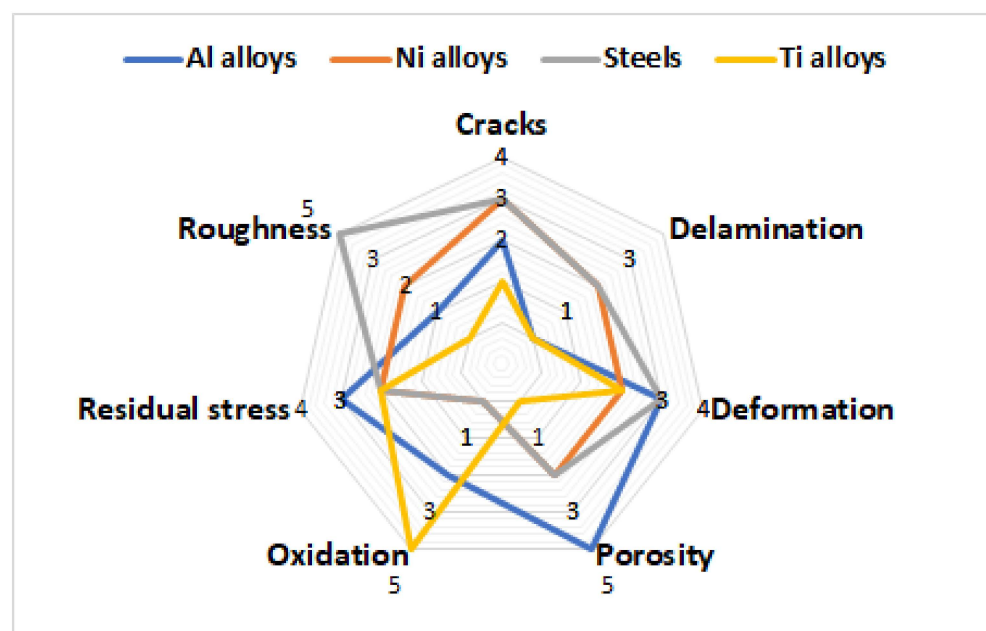


Figure 4. The correlation between materials and defects in WAAM processes.

They explored the grain size and morphology in three alloy systems. The first alloy investigated was Ti-6Al-4V, which contains no added grain refiners or nucleant particles (low Q solutes). The second alloy was Ti-3Al-8V-6Cr-4Mo-4Zr, a high Q alloy containing growth-restricting solute (Cr has a high Q in titanium) and no added nucleant particles. The third alloy, Ti-3Al-8V-6Cr-4Mo-4Zr + La₂O₃, contained both growth restriction solute and added nucleant particles. According to the results of Bontha et al. [49], the Ti64 (Ti-6Al-4V) alloy produced a very large mixed equiaxed-columnar grain morphology. In the second alloy, the presence of grain-refining solutes refined the grain size by 55% mainly by narrowing the width of the columnar grain but failed to produce a more important fraction of equiaxed grain. However, the addition of nucleant particles (La₂O₃) produced columnar grains at the base and equiaxed zone at the top of the layer and refined the grain size by 85%. The La₂O₃ particles seem to act as heterogeneous nucleation sites. The temperature gradients decrease during layer solidification, which provides constitutional supercooling and equiaxed grain nucleation. Thus, interpass cooling during wire-based additive manufacturing could reduce the temperature gradients and help constitutional supercooling to occur. The effect of the interpass cooling process was studied by Ding et al. [27] in order to generate material with better mechanical properties than standard WAAM on Ti-6Al-4V alloy. The study has shown that, besides improving microhardness and tensile strength due to the refinement of the lamellar α structure, using active interpass cooling significantly reduces adverse thermal effects and thus creates uniform microstructures in the deposition. However, the grain size has not noticeably changed. Recently, Zhang et al. [31], in order to promote CET of titanium grains, developed a titanium–copper alloy Ti-8.5 Cu that has a high constitutional supercooling capacity. By exploring binary titanium alloy phase diagrams, they noted that copper could be a promising solute with a high Q value and therefore a good grain refiner (for refining β -phase titanium grains). In addition, copper is a eutectoid-forming element where $\beta \rightarrow \alpha + \text{Ti}_2\text{Cu}$ in titanium binary alloy systems at 790 °C and diffuses rapidly into titanium, which is important (due to the high cooling rate of the process) to establish a sufficiently large constitutional supercooling zone in front of the solid–liquid interface. They also showed that faster higher constitutional supercooling delivered by more copper solute, and therefore it reduced the equiaxed β grain size with increasing copper content. This approach to grain refinement, using alloys with high Q values, has been demonstrated through many alloying systems. The identification and characterization of these solutes is the subject of ongoing work, but the results achieved so far are promising to optimize the quality of WAAM-fabricated components.

5. Nucleant Particles for Grain Refinement

The outcome of the local solidification of the small melt pools in titanium alloys during layer deposition is the formation of columnar grains and epitaxial growth as heat is primarily extracted through the previously deposited solidified layer, often across a steep thermal gradient [19]. The appearance of an α -grain boundary, which develops during subsequent solid-state transformation along the aligned prior β columnar grains, can lead to poor ductility and highly anisotropic properties in components produced by AM [34,39,67–69]. The issue of large directional grains can be addressed either with the addition of a solute that promotes constitutional supercooling, potent nuclei, or both [70,71]. The interdependence model clearly shows the interdependence between the potential of the solute and particle to form an equiaxed structure. Nuclei as the grain starting points are initially present in liquid metals. The introduction of additional nucleant particles by inoculation facilitates grain refinement by increasing the total number of grains and therefore reducing the average grain size [72]. Selective growth-limiting solutes can enhance grain refinement by providing the necessary supercooling to activate nucleant particles. Parallel to the direction of heat transfer from a pre-existing solid region, columnar grain growth occurs. To facilitate grain refinement and to obtain homogeneity, this phenomenon must be restricted. Constitutional melt pool supercooling reduces the growth rate of columnar grains at the solid–liquid interface [70]. This allows additional nucleation events

to take place within the melt pool as a result of increasing the density of grain. Grain refinement can be optimized to produce many nucleation events, by using a solute in unison and potent nuclei.

Tedman-Jones et al. [73] investigated the effect of adding Mo, Nb, and W particles as potential nucleants in a WAAM titanium alloy. The aforementioned particles were found to be stable enough to withstand melting during solidification and to act as strong substrates for β -grain growth, facilitating the formation of equiaxed grains. They have proposed that the inoculant particles were slightly dissolved and enriched the surrounding liquid in the melting process and the rich boundary led to growth from the particle surface.

Birmingham [74] used trace boron particles in distinguished amounts of Ti-6Al-4V alloy produced by WAAM. It was observed a significant change in β columnar grains morphology to a narrower structure and plasticity improvement without compression strength loss. On the other hand, a wider range of solidification and freezing was represented as a result of the presence of boron particles. It asserted the role of boron particles in α equiaxed grains chiefly after heat treatment with the help of TiB needles and their role in α -phase nucleation.

Birmingham et al. [75] investigated the effect of lanthanum hexaboride (LaB₆) particles on grain structure, anisotropy, and shape of the melt pool. Ti-6Al-4V wire was used for the deposit as the feedstock. The alloying of lanthanum changed the molten pool shape and also produced TiB compounds, which made constraints on growth in the lateral direction during solidification and consequently thinner columnar grains.

Merreddy et al. [9] applied silicon as a refining additive to a WAAM titanium-fabricated component with the aim of reducing the grain size. Silicon was able to decrease the columnar grain width by restricting the growth mechanism. They have found that without using other effective refiners, silicon can only make the grains narrower and could not have a major impact on the grain size.

Birmingham et al. [34], with the aim of different alloy composition impacts on columnar-to-equiaxed transition (CET), compared three situations of using alloying elements in the Ti6Al4V wire arc additively manufactured process. They defined three alloy compositions: an alloy with no additives; an alloy with Zr, Mo, and Cr grain refiners; and an alloy with grain refiners containing La₂O₃ nucleant particles. They have reported considerable grain refinement and equiaxed structure attainment with the third one. They believed that La₂O₃ nucleant particles played an effective role as nucleation sites.

To reduce the grain size of the β -Ti in a Ti-6Al-4V WAAM component, Kennedy [76] used ZrN and TiN phases as inoculants. The observation demonstrated the effectiveness of TiN particles in grain refining, while the ZrN failed to meet expectations. The effective role of TiN clusters as nucleation centers is expressed as the reason.

Because of the power of carbon in alloying of Ti alloys, Merreddy et al. [77] applied trace carbon in WAAM manufacturing with Ti-6Al-4V. In microstructure exploration, they have found that adding near 0.4 wt.% carbon reduced the grain size due to increasing the grain density. During the solidification, carbon caused supercooling and subsequently restricted the growth that makes finer grains.

6. Post-Processing of WAAM Parts

Usually, to improve the material properties of WAAM parts, post-process treatment, such as reducing surface roughness and porosity or removing stress and distortions, is required. For WAAM Ti parts, the most severe defects are oxidation, deformation, and residual stress (see Figure 4). For other alloys, Table 3 presents the tendency of various defects in WAAM-fabricated parts. With appropriate post-processing, most issues that influence deposition quality can be reduced or eliminated. Nowadays, to improve part quality in the WAAM process, several post-process treatment technologies have been reported. This section will review these techniques, both their limitations and features.

Table 3. Tendency of various defects in WAAM-fabricated parts. The data is reproduced with permission from authors in [20,78].

Material	Process	Defect or Feature					
		Porosity	Cracking	Delamination	Oxidation	Substrate Adherence	Surface Finish
Ti6Al4V	TIG	No	No	No	Light	Good	Smooth
	Plasma	No	No	No	No	Good	Smooth
	CMT	No	No	No	Light	Good	Smooth
	DCEP-GMAW	No	No	No	Light	Medium	Poor
H08Mn2Si steel	DE-GMAW	Low	No	No	No	Good	Waviness
Copper-coated steel	GMAW	No	No	No	Light	Good	Medium-rough
	CMT	High	No	No	Light	Good	Smooth
ER4043 Al alloy	VP-GTAW	No	No	No	No	Good	Medium-rough
	CMT	High	No	No	No	Good	Smooth
AA2319 Al alloy	CMT-PADV	No	No	No	No	Good	Smooth
	VP-GTAW	No	Yes	No	No	Good	Smooth
5356 Al alloy	VP-GTAW	No	Yes	No	No	Good	Smooth
Inconel 625	PPAD	High	Yes	No	No	Good	Smooth
	GTAW	No	No	No	No	Good	Smooth
Inconel 718	GMAW	Medium	Yes	Yes	No	Good	Smooth
AZ31 Mg alloy	PMIG	No	No	No	Light	Medium	Medium-rough
Nickel-Al-Cu	CMT	No	No	No	No	Good	Smooth
Steel-bronze bimetal	GMAW	No	No	No	No	Good	Smooth
Steel-nickel bimetal	GMAW	No	No	No	No	Good	Medium-rough
Intermetallic Fe/Al	GTAW	High	Yes	No	Serious	Medium	Medium-poor
Intermetallic Al/Ti	GTAW	Low	Yes	No	No	Good	Rough
Intermetallic Al/Cu	GTAW	No	No	Yes	Light	Poor	Rough

6.1. Post-Process Heat Treatment

Post-process heat treatment is widely used in WAAM to reduce residual stress, improve material strength, and control material hardness. Proper heat treatment depends on the AM methods, working temperature, and target material. The cracking probability under mechanical loading will increase if the heat treatment state is set incorrectly [36]. As summarized in Figure 5, after heat treatment, the mechanical strength of WAAM-fabricated parts improved significantly, with an increase of up to 6% in UTS and YS being reported for titanium alloy Ti6Al4, respectively. Moreover, post-process heat treatment plays an important role in grain refinement, especially for WAAM-fabricated Inconel and aluminum alloy [79].

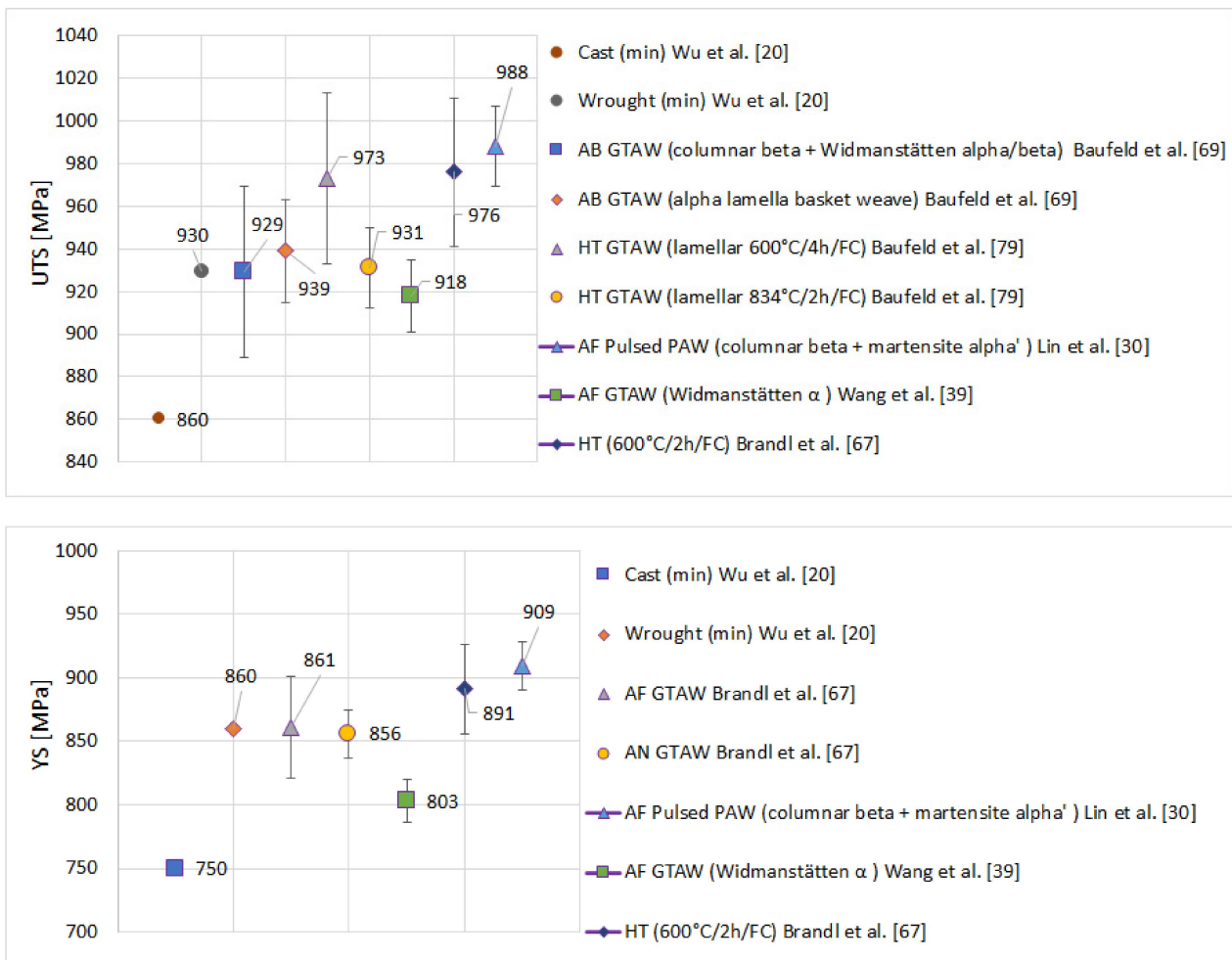


Figure 5. Mechanical properties (in build direction, ultimate tensile strength (UTS), and yield strength (YS)) of Ti-6Al-4V-fabricated from various WAAM processes (AF: as fabricated, HT: heat treated, GTAW: gas tungsten arc welding, PAW: plasma arc welding).

6.2. Interpass Cold Rolling

As previously mentioned, the WAAM process induces anisotropic mechanical properties and microstructural evolution due to the thermal gradient with deposition layers and alternate reheating and recooling processes. The cold-rolling technique is able to reduce microstructural anisotropy by plastically deforming the deposition. A roller is used to refine the microstructure and enhance tensile strength in the longitudinal direction [80]. Both tensile strength and yield strength in the build direction are improved through interpass cold rolling. Thus, this technique contributes to having a more homogeneous microstructure, therefore mechanical properties in the target component. However, this technique is more suitable for simple deposited parts due to the geometrical limitation of the rolling process. If the component is more complex, with curves and corners, special flexible tooling is needed to achieve an effective rolling process, increasing the cost of the process and thus reducing the range of industrial applications.

6.3. Interpass Cooling

More recently, interpass cooling for WAAM has been developed [81]. There is a gas nozzle (supplied with argon, nitrogen, or CO₂) used to provide active cooling during the fabrication after the deposition of each layer. The in-situ layer temperature can be controlled and thereby the microstructure and mechanical properties. This process still needs some investigation. It could also reduce residual stress and deformation, even if it

has not been proven yet. Wu et al. [81] found that interpass cooling on WAAM-fabricated Ti-6Al-4V parts produces less oxidation, a refined structure, and improved hardness and strength. Moreover, manufacturing efficiency is improved due to the reduction of dwell time between deposited layers. Thus, interpass cooling is a very promising technology to improve WAAM processes.

6.4. Peening and Ultrasonic Impact Treatment

Ultrasonic impact treatments (UITs) and peening both are cold mechanical treatments that are used to improve mechanical properties by reducing local residual stress in welding applications. By imposing compressive stress in these techniques, the surface of the weld releases tensile stress. Ultrasonic impact treatment produces grain refinement and randomizes orientations, which contributes to mechanical strength improvement. It has been reported [82] that the microhardness of Ti-6Al-4V WAAM-fabricated parts can be increased by 28%, and the surface residual stress can be reduced to 58% compared to the untreated sample after ultrasonic impact treatment. The surface-modified layers with significant grain refinement are up to 60 μm below the surface; therefore, both techniques have a negligible effect on the internal residual stresses of large metal parts fabricated using WAAM.

6.5. In-Process Ultrasonic Vibration Treatment

Ultrasonic vibration (UV) is used for casting [83] and welding [84] to improve mechanical characteristics and to reduce defects such as porosity. UV has been recently investigated in laser-based DED [85] using different materials, including nickel-based [85,86] and Ti-based alloys [87]. Similar to peening, UV has an impact on grain refinement but also on porosity and chemical homogenization, especially at the interface between two materials. The vibration has an effect on the molten pool by leading to acoustic cavitation and agitation at the interface liquid–solid during solidification. Consequently, the dispersion of crystals at the interface leads to a finer microstructure with equiaxed grains promoting globular grains instead of large dendrite growth. It has been reported that grain refinement and the reduction of porosity had an impact on microhardness [85] and tensile properties [87]. However, the sonotrode fixed with the substrate is initially in resonance with the ultrasonic transducer. During manufacturing of the part, the height will vary layer after layer. It has an impact on the resonance condition and consequently on the acoustic cavitation. Alternative technology, such as a magnetostrictive transducer, has been proposed to overcome this problem but is dependent on the selected material [87].

Recent research has not reported the use of UV with the WAAM process, and it is yet to be explored [78]. As extensively explored in LB-PBF, the melt pool is affected by increasing energy density as it gets wider, deeper, and more asymmetrical [88–91]. Such differences in the heat input and the melt pool size could have an impact on the grain refinement. Moreover, an evaluation of the cavitation depending on the height of the part is necessary. An innovative approach should be proposed to resolve these limitations.

7. Modeling of Solidification Microstructure

Modeling of the solidification microstructure typically begins with a numerical thermal model to determine the temperature field in the fusion zone and continues by determining thermal gradients and cooling rates with associated solidification parameters. For obtaining thermal fields, geometry of the fusion zone, lack of fusion, and heating/cooling rates, possible numerical methods include the discrete element method (DEM), smoothed particle hydrodynamics (SPH), the finite-element method (FEM), and computational fluid dynamics (CFD). Knowledge gaps in fusion zone and melt pool simulations exist. To represent melt pool dynamics accurately, temperature-dependent surface tension and wetting forces, Marangoni effects, and evaporation-induced recoil pressure need to be taken into account. Most models do not consider the evolution of the solid phase and fluid–solid interactions in the melt pool and/or lack a realistic heat source model with experimental validation.

The kinetics of solidification, nucleation, grain growth, texture, solid-state phase transformation, and the resultant microstructure can be predicted using different sets of numerical microstructure evolution models. There are three most common methods used for modeling solidification science: (i) phase field (PF) method, (ii) Monte Carlo (MC) method, and (iii) cellular automata (CA) method. The most commonly used numerical models for metal additive manufacturing, their outcomes, and their highlights are classified and given in Table 4 [92].

Table 4. Classification of numerical models. Adopted from the data presented in [92].

Aim	Model	Highlights	Outcomes
Heat transfer numerical analysis	Heat conduction model [89,90]	3D heat conduction equation is solved numerically using FEM/FDM methods	Thermal field, geometry of fusion zone, heating/cooling rates
	Heat conduction–convection model	3D transient solution for conservation of mass, momentum, and energy	Thermal and velocity fields, geometry of fusion zone, lack of fusion, heating/cooling rates
	Volumetric fluid flow model	Free surface of fusion zone movement	Thermal and velocity fields, heating/cooling rates
Microstructure, nucleation, grain growth	Time-temperature-transformation [93], Continuous cooling transformation [93], Johnson–Mehl–Avrami model [94]	Kinetics of phase transformation during cooling	Solid-state phase transformation kinetics
	Phase field method [95–99]	Calculation of an order parameter based on free energy to represent the state of entire microstructure	Evolution of phases, nucleation, grain growth, solid-state phase transformation
	Monte Carlo method [100–102]	Probabilistic method for grain orientation change	Solidification microstructure, grain growth, texture
	Cellular automata [100–103]	Element birth and death for calculating grain growth and subgrain structure	Solidification microstructure, grain growth, texture

7.1. Phase Field Method

The PF method’s main advantage is that due to its continuous-order parameters, it avoids the explicit tracking of the solid–liquid interface whose location is unknown [95,96]. It allows the direct representation of curvatures and grain boundaries, which is difficult to achieve with CA and MC models [97]. It represents arbitrary particle morphology without making any assumptions about particle shape [97]. It provides excellent capabilities for describing and simulating the solidification process and dendritic growth [98].

Disadvantages include (i) limited to use in homogeneous deformation [97]; (ii) requiring a lot of computational work, which is inefficient and time-consuming [97]; and (iii) being based on small length scales and can only simulate a few grains. These small-scale simulations are not representative of AM processes, which commonly involve hundreds or thousands of layers and scan passes [98]. It contains a large number of phenomeno-

logical parameters related to the thermodynamic properties, the phase composition, the interfacial structure, the diffusion of solute elements, and the elastic/plastic properties of the coexisting phases; meanwhile, most of these parameters are difficult to measure [100].

7.2. Monte Carlo Method

Advantages include (i) simple numerical model with easy implementation [97]; (ii) very low calculation cost and ability to predict 3D microstructures with hundreds of heat source passes [98,101]; and (iii) achievable information on the grain size change, observable evolution of grain morphology, and obtainable mechanism of grain growth [97]. Drawbacks include (i) no random or deterministic transformation rule in the MC approach [97]; (ii) state variable of MC is updated at each subsequent time step interval, while in the CA method, all the cells are updated synchronously [98]; (iii) it does not really reflect the mechanism of grain boundary change, and the obtained grain growth index is quite different from the theoretical grain growth index [97]; (iv) there is a nontrivial correlation between the time and length of simulation and the physical time and length, which needs to be scaled or matched with experimental data [97,100]; (v) it does not incorporate a crystallographic texture prediction [98] or anisotropy [97] (of additive manufactured material [101]); (vi) it cannot simulate solid-state phase transformation [102]; (vii) it does not account for the effect of temperature accumulation during the addition of layers on melt pool geometry (i.e., not suitable for thin wall structures) [97]; and (viii) it does not allow for direct coupling of thermal and microstructure models [102].

7.3. Cellular Automata Method

The CA method requires fewer computer resources because the discrete nature of the algorithms is well suited for parallelization and therefore allows for simulations of a large number of grains within domains at the millimeter scale. Advantages are (i) due to the part on definite evolution of grain growth in CA method, the steps used in CA are less than MC method, so the computational efficiency of the CA method is increased in comparison with the MC method [96]; (ii) at each time interval, it updates the variable values simultaneously for all cells according to CA rules, which depend on the physical model of the system [97] in contrast to the MC methods, where one evaluated lattice point is randomly selected in each MCS when considering a change in its state [96]; (iii) compared with PF, the CA method requires fewer computer resources because the discrete nature of the algorithms is well suited for parallelization and therefore allows for simulations of a large number of grains within domains at the millimeter scale [100,103]; (iv) simple local rules and discrete methods can be used to describe complex physical phenomena and morphologies resulting from local interactions [97]; (v) curvature-driven mechanisms, thermodynamic-driven mechanisms, and energy dissipation mechanisms are introduced in local transformation rules, which can more realistically reflect the physical process of grain boundary migration [97]; (vi) enables crystallographic texture prediction [98]; and (vii) simulates solid-state diffusional phase transformation [98,100].

Disadvantages include (i) compared with PF, the CA method cannot capture fine details of the dendrite network [103]; (ii) the CA mesh can introduce artificial anisotropy [98]; (iii) the accuracy of the model is dependent on cell size [98]; (iv) a precise calculation of the mean curvature, which is necessary for grain boundary migration by capillarity, is difficult [102]; (v) due to the sharp interface, CA is less accurate in predicting solid-state diffusional phase transformation than the phase-field models with the diffuse interface [100]; (vi) for solid-state diffusional phase transformations, the time step is virtual or defined as, e.g., the ratio between the cell size and maximum interface velocity, or a scaled ratio between the average cell size and the average interface velocity, which is deficient in physical meanings [100]; and (vii) free open-source code is currently unavailable [102].

8. Combined Mechanistic and Data-Driven Modeling

WAAM processes are dependent on multiple simultaneously occurring physical processes, which are often hard to predict and optimize simultaneously. Design of experiments (DoE) is a traditional method to explore the combinations of process parameters that lead to optimal results. For example, weld-bead dimensions and penetration depth were modeled using fractional and Taguchi-inspired DoE [104], allowing the predictability of both high penetration and wide-bead welds suitable for root passes Ti-6-4 and Inconel-718.

Grain refinement in WAAM has been modeled using exploratory DoE, which included a fixed set of process parameters and involved modifying bulk chemical compositions to study solidification microstructures comprising large cm scale <001> fiber-textured and columnar β grains, which are detrimental to mechanical performance [105].

Recent literature on AM points to a trend that combines mechanistic models and machine learning to predict process parameters that will improve part quality, lower cost, and reduce the volume of trial-and-error experiments for qualifying parts [92].

Combining mechanistic models and machine learning proves to be suitable to create meta-analysis methods capable of predicting the evolution of the microstructures, properties, and defects in metal AM, for example, to predict processing conditions to achieve desired microstructure and properties such as grain size, distribution and orientation, tensile strength, hardness, and fatigue life [106,107]. Neural-network-based machine learning examples [107] show the ability to predict microstructure and understand the processing structure–property relationship for the PBF process, showing comparable results with the more computationally intensive Monte Carlo method [103].

Although progress has been made in quantifying microstructural features using machine learning, the applications of machine learning to control microstructure and properties during metal printing remain in their initial stages of development [92].

9. Summary and Future Outlook

The desire for traditional manufacturing reconsideration, increasing production capacity and quality demand, waste-reducing tendency, and using machine learning in industries with dead heat races point to additive manufacturing growth in the foreseeable future. The average growth of additive manufacturing was over 27% in the past decade, and it grew by 7.5% to nearly USD 12.8 billion in 2020. The striking point is a 7% growth in less-established firms despite the COVID-19 pandemic [108]. The engineering of alloys such as steels and Al, Ni, and Ti alloys relevant to many industries is already employed in WAAM with powerful results, demonstrating the viability of this DED AM method to deliver not only cost-effective but also custom-made large metallic parts. Some applications using WAAM-manufactured parts are present in the market, and it is expected that industry will perform a critical task in expanding the applications of WAAM parts. The literature on WAAM additive manufacturing points to undeniable trends. In the first part, the history of the various types of wire arc additive manufacturing, the advantages of using this method in comparison with other 3D printing processes, and its unmistakable role in producing large, precious components in industry are demonstrated. In the second part, the significance of the microstructure, grain size, and morphology and their impact on the mechanical properties of the AM-fabricated parts is depicted. Any enhancement or modification to this intrinsic characteristic will affect the serviceability of the products. The third part implies the influence of using alloying particles, process control, and post-processing on the final microstructure and consequently the mechanical properties. It points to recent studies on various procedures with the aim of grain refinement. Last, the paper insists on the irrefutable consequences of smart prediction of the material manner by using computer programs, modeling, and simulation.

10. Research Directions

Based on the discussions in this review paper, the research directions can be given in the research challenges: (1) microstructure grain refinement to obtain a fine equiaxed $\alpha + \beta$ structure, eliminating the anisotropy property and improving the overall properties; and (2) physics-based simulation modeling for solidification microstructure prediction. Fundamentally, the following questions should be answered:

- Could the research improve the properties of additively manufactured titanium alloy by grain refinement of the product using a combination of the three main optimized solutions (alloying element changing, adding nucleants, using mechanical means, and changing the process parameters)?
- Does reducing defects by controlling the process parameters and feedstock quality help the grain refinement and hence improve the properties, or does their presence during solidification help to obtain a finer microstructure?
- Is phase and microstructure refinement effective and profitable for the corrosion resistance properties of the products?
- What is the effect of the grain size, shape, and microstructure on the surface roughness and integrity?
- How can physics-based simulation modeling for solidification microstructure and grain morphology describe the optimized condition for the aforementioned process?

The first research direction could be to determine the challenges for obtaining an equiaxed fine-grained microstructure from a coarse columnar structure. This would provide a preliminary experimental understanding of the effects of chemical composition and process parameters on the size and shape of the grains and the microstructure of titanium alloys additively manufactured with the powder bed fusion method. These studies should demonstrate that the addition of additives is effective in refining the microstructure of AM titanium components. The impact of the addition of Si, B, Al, V, W, and Be on the width of the columnar grains and whether it allows for the nucleation of some equiaxed grains through the development of constitutional supercooling and growth restriction should be investigated. Furthermore, the effect of mechanical and process parameters that changed the shape and size of the microstructure should be examined. An attentive examination of the factors affecting the final structure is crucial to determine an optimal method.

The second research direction could be to refine the grain structure by using alloying elements and nucleant nanoparticles. This would determine the optimized chemical composition by evaluating the microstructure using an optical/polarized microscope and SEM to characterize the optimum structure with the aim of the $\alpha + \beta$ fine-grained equiaxed microstructure. The microstructure and macrostructure of the samples should be characterized by optical microscopy techniques, and phases should be analyzed by using SEM to ensure the optimum structure. The grain size should be measured with image analysis software according to ASTM E112 and should be compared with other studies.

The next step will be metallography experiments on feedstock and final-component micro-defects to determine the main source of the defects, which would be the powders, in-process, or both. The microstructure characterization of the source powders/wires will be examined before the AM process. Their effect (positive or negative) on the solidification and grain morphology of the product will be demonstrated.

The next research direction is the study of the microstructure refinement effect on the physical, mechanical, and corrosion resistance properties. This will yield the results of mechanical, physical, and corrosion tests and comparisons with recent studies on the same alloys. For investigations on the mechanical and physical properties, as well as tensile, micro- and macro-hardness, and corrosion properties, compatible corrosion test methods such as the Tafel technique or intergranular corrosion attack should be implemented.

Author Contributions: Conceptualization, T.Ö.; methodology, T.Ö. and H.S.; formal analysis, H.S. and R.L.; resources, T.Ö.; data curation, T.Ö. and R.L.; writing—original draft preparation, R.L. and H.S.; writing—review and editing, H.S. and T.Ö.; visualization, T.Ö.; supervision, T.Ö. All authors have read and agreed to the published version of the manuscript.

Funding: This research received no external funding.

Conflicts of Interest: The authors declare no conflict of interest.

References

1. Fu, R.; Tang, S.; Lu, J.; Cui, Y.; Li, Z.; Zhang, H.; Xu, T.; Chen, Z.; Liu, C. Hot-wire arc additive manufacturing of aluminum alloy with reduced porosity and high deposition rate. *Mater. Des.* **2021**, *199*, 109370. [[CrossRef](#)]
2. Aldalur, E.; Veiga, F.; Suárez, A.; Bilbao, J.; Lamikiz, A. High deposition wire arc additive manufacturing of mild steel: Strategies and heat input effect on microstructure and mechanical properties. *J. Manuf. Process.* **2020**, *58*, 615–626. [[CrossRef](#)]
3. Taminger, K.M.; Domack, C.S. Challenges in Metal Additive Manufacturing for Large-Scale Aerospace Applications. In *Women in Aerospace Materials; Women in Engineering and Science*; Kinsella, M., Ed.; Springer: Cham, Switzerland, 2020; pp. 105–124. [[CrossRef](#)]
4. Ahn, D.-G. Directed Energy Deposition (DED) Process: State of the Art. *Int. J. Precis. Eng. Manuf. Green Technol.* **2021**, *8*, 703–742. [[CrossRef](#)]
5. Xia, C.; Pan, Z.; Polden, J.; Li, H.; Xu, Y.; Chen, S.; Zhang, Y. A review on wire arc additive manufacturing: Monitoring, control and a framework of automated system. *J. Manuf. Syst.* **2020**, *57*, 31–45. [[CrossRef](#)]
6. Dugar, J.; Ikram, A.; Klobčar, D.; Pušavec, F. Sustainable Hybrid Manufacturing of AlSi5 Alloy Turbine Blade Prototype by Robotic Direct Energy Layered Deposition and Subsequent Milling: An Alternative to Selective Laser Melting? *Materials* **2022**, *15*, 8631. [[CrossRef](#)]
7. Ding, D.; Pan, Z.; Cuiuri, D.; Li, H. Wire-feed additive manufacturing of metal components: Technologies, developments and future interests. *Int. J. Adv. Manuf. Technol.* **2015**, *81*, 465–481. [[CrossRef](#)]
8. Williams, S.W.; Martina, F.; Addison, A.C.; Ding, J.; Pardal, G.; Colegrove, P. Wire + Arc Additive Manufacturing. *Mater. Sci. Technol.* **2016**, *32*, 641–647. [[CrossRef](#)]
9. Mereddy, S.; Bermingham, M.J.; StJohn, D.H.; Dargusch, M.S. Grain refinement of wire arc additively manufactured titanium by the addition of silicon. *J. Alloys Compd.* **2017**, *695*, 2097–2103. [[CrossRef](#)]
10. Childerhouse, T.; Jackson, M. Near Net Shape Manufacture of Titanium Alloy Components from Powder and Wire: A Review of State-of-the-Art Process Routes. *Metals* **2019**, *9*, 689. [[CrossRef](#)]
11. Sebbe, N.P.V.; Fernandes, F.; Sousa, V.F.C.; Silva, F.J.G. Hybrid Manufacturing Processes Used in the Production of Complex Parts: A Comprehensive Review. *Metals* **2022**, *12*, 1874. [[CrossRef](#)]
12. Pragana, J.P.M.; Sampaio, R.F.V.; Bragança, I.M.F.; Silva, C.M.A.; Martins, P.A.F. Hybrid metal additive manufacturing: A state-of-the-art review. *Adv. Ind. Manuf. Eng.* **2021**, *2*, 100032. [[CrossRef](#)]
13. Alonso, U.; Veiga, F.; Suárez, A.; Del Val, A.G. Characterization of Inconel 718[®] superalloy fabricated by wire Arc Additive Manufacturing: Effect on mechanical properties and machinability. *J. Mater. Res. Technol.* **2021**, *14*, 2665–2676. [[CrossRef](#)]
14. Kindermann, R.M.; Roy, M.J.; Morana, R.; Prangnell, P.B. Process response of Inconel 718 to wire + arc additive manufacturing with cold metal transfer. *Mater. Des.* **2020**, *195*, 109031. [[CrossRef](#)]
15. Artaza, T.; Bhujangrao, T.; Suárez, A.; Veiga, F.; Lamikiz, A. Influence of heat input on the formation of laves phases and hot cracking in plasma arc welding (PAW) additive manufacturing of inconel 718. *Metals* **2020**, *10*, 771. [[CrossRef](#)]
16. Lopes, J.G.; Machado, C.M.; Duarte, V.R.; Rodrigues, T.A.; Santos, T.G.; Oliveira, J.P. Effect of milling parameters on HSLA steel parts produced by Wire and Arc Additive Manufacturing (WAAM). *J. Manuf. Process.* **2020**, *59*, 739–749. [[CrossRef](#)]
17. Zhang, H.; Huang, J.; Liu, C.; Ma, Y.; Han, Y.; Xu, T.; Lu, J.; Fang, H. Fabricating Pyramidal Lattice Structures of 304 L Stainless Steel by Wire Arc Additive Manufacturing. *Materials* **2020**, *13*, 3482. [[CrossRef](#)]
18. Veiga, F.; Suárez, A.; Aldalur, E.; Goenaga, I.; Amondarain, J. Wire Arc Additive Manufacturing Process for Topologically Optimized Aeronautical Fixtures. *3D Print. Addit. Manuf.* **2021**. [[CrossRef](#)]
19. Antony, A.A.; Meyer, J.; Prangnell, P.B. Effect of build geometry on the β -grain structure and texture in additive manufacture of Ti6Al4V by selective electron beam melting. *Mater. Charact.* **2013**, *84*, 153–168. [[CrossRef](#)]
20. Wu, B.; Pan, Z.; Ding, D.; Cuiuri, D.; Li, H.; Xu, J.; Norrish, J. A review of the wire arc additive manufacturing of metals: Properties, defects and quality improvement. *J. Manuf. Process.* **2018**, *35*, 127–139. [[CrossRef](#)]
21. Dhinakaran, V.; Ajith, J.; Fahmidha, A.F.Y.; Jagadeesha, T.; Sathish, T.; Stalin, B. Wire Arc Additive Manufacturing (WAAM) process of nickel based superalloys—A review. *Mater. Today Proc.* **2020**, *21*, 920–925. [[CrossRef](#)]
22. Totin, A.; MacDonald, E.; Conner, B.P. Additive Manufacturing for Aerospace Maintenance and Sustainment (Postprint) Air Force Research Laboratory Materials and Manufacturing Directorate Wright-Patterson Air Force Base, Oh 45433-7750 Air Force Materiel Command United States Air Force. 2019. Available online: www.dsiac.org (accessed on 14 December 2022).
23. Sames, W.J.; List, F.A.; Pannala, S.; Dehoff, R.R.; Babu, S.S. The metallurgy and processing science of metal additive manufacturing. *Int. Mater. Rev.* **2016**, *61*, 315–360. [[CrossRef](#)]

24. Reichardt, A.; Dillon, R.P.; Borgonia, J.P.; Shapiro, A.A.; McEnerney, B.W.; Momose, T.; Hosemann, P. Development and characterization of Ti-6Al-4V to 304L stainless steel gradient components fabricated with laser deposition additive manufacturing. *Mater. Des.* **2016**, *104*, 404–413. [CrossRef]
25. Procada, Directed Energy Deposition Additive Manufacturing. 2023. Available online: <https://www.procada.se/technology.html> (accessed on 14 December 2022).
26. Sciaky, Additive Manufacturing. 2022. Available online: <https://www.sciaky.com/additive-manufacturing/electron-beam-additive-manufacturing-technology> (accessed on 14 December 2022).
27. McAndrew, A.R.; Rosales, M.A.; Colegrove, P.A.; Hönnige, J.R.; Ho, A.; Fayolle, R.; Eytayo, K.; Stan, I.; Sukrongpang, P.; Crochemore, A.; et al. Interpass rolling of Ti-6Al-4V wire + arc additively manufactured features for microstructural refinement. *Addit. Manuf.* **2018**, *21*, 340–349. [CrossRef]
28. Özel, T.; Altay, A.; Donmez, A.; Leach, R. Surface topography investigations on nickel alloy 625 fabricated via laser powder bed fusion. *Int. J. Adv. Manuf. Technol.* **2018**, *94*, 4451–4458. [CrossRef]
29. Asala, G.; Khan, A.K.; Andersson, J.; Ojo, O.A. Microstructural Analyses of ATI 718Plus[®] Produced by Wire-ARC Additive Manufacturing Process. *Metall. Mater. Trans. A* **2017**, *48*, 4211–4228. [CrossRef]
30. Lin, J.; Lv, Y.; Liu, Y.; Sun, Z.; Wang, K.; Li, Z.; Wu, Y.; Xu, B. Microstructural evolution and mechanical property of Ti-6Al-4V wall deposited by continuous plasma arc additive manufacturing without post heat treatment. *J. Mech. Behav. Biomed. Mater.* **2016**, *69*, 19–29. [CrossRef]
31. Zhang, D.; Qiu, D.; Gibson, M.A.; Zheng, Y.; Fraser, H.L.; StJohn, D.H.; Easton, M.A. Additive manufacturing of ultrafine-grained high-strength titanium alloys. *Nature* **2019**, *576*, 91–95. [CrossRef]
32. Zhang, D.; Prasad, A.; Birmingham, M.J.; Todaro, C.J.; Benoit, M.J.; Patel, M.N.; Qiu, D.; StJohn, D.H.; Qian, M.; Easton, M.A. Grain Refinement of Alloys in Fusion-Based Additive Manufacturing Processes. *Metall. Mater. Trans. A* **2020**, *51*, 4341–4359. [CrossRef]
33. Collins, P.C.; Haden, C.V.; Ghamarian, I.; Hayes, B.J.; Ales, T.; Penso, G.; Dixit, V.; Harlow, G. Progress toward an integration of process–structure–property–performance models for “three-dimensional (3-D) printing” of titanium alloys. *JOM* **2014**, *66*, 1299–1309. [CrossRef]
34. Birmingham, M.J.; StJohn, D.H.; Krynen, J.; Tedman-Jones, S.; Dargusch, M.S. Promoting the columnar to equiaxed transition and grain refinement of titanium alloys during additive manufacturing. *Acta Mater.* **2019**, *168*, 261–274. [CrossRef]
35. Chen, Y.; Yang, C.; Fan, C.; Zhuo, Y.; Lin, S.; Chen, C. Grain refinement of additive manufactured Ti-6.5Al-3.5Mo-1.5Zr-0.3Si titanium alloy by the addition of La₂O₃. *Mater. Lett.* **2020**, *275*, 128170. [CrossRef]
36. Ng, C.H.; Birmingham, M.J.; Dargusch, M.S. Controlling grain size, morphology and texture in additively manufactured β -titanium alloy with super transus hot isostatic pressing. *Addit. Manuf.* **2022**, *59*, 103176. [CrossRef]
37. Yuan, D.; Shao, S.; Guo, C.; Jiang, F.; Wang, J. Grain refining of Ti-6Al-4V alloy fabricated by laser and wire additive manufacturing assisted with ultrasonic vibration. *Ultrason. Sonochem.* **2021**, *73*, 105472. [CrossRef]
38. Lu, T.; Liu, C.; Li, Z.; Wu, Q.; Wang, J.; Xu, T.; Liu, J.; Wang, H.; Ma, S. Hot-wire arc additive manufacturing Ti-6.5Al-2Zr-1Mo-1V titanium alloy: Pore characterization, microstructural evolution, and mechanical properties. *J. Alloys Compd.* **2020**, *817*, 153334. [CrossRef]
39. Wang, F.; Williams, S.; Colegrove, P.; Antonysamy, A.A. Microstructure and mechanical properties of wire and arc additive manufactured Ti-6Al-4V. *Metall. Mater. Trans. A* **2013**, *44*, 968–977. [CrossRef]
40. Lervåg, M.; Sørensen, C.; Robertstad, A.; Brønstad, B.M.; Nyhus, B.; Eriksson, M.; Aune, R.; Ren, X.; Akselsen, O.M.; Bunaziv, I. Additive Manufacturing with Superduplex Stainless Steel Wire by CMT Process. *Metals* **2020**, *10*, 272. [CrossRef]
41. Stützer, J.; Totzauer, T.; Wittig, B.; Zinke, M.; Jüttner, S. GMAW Cold Wire Technology for Adjusting the Ferrite–Austenite Ratio of Wire and Arc Additive Manufactured Duplex Stainless Steel Components. *Metals* **2019**, *9*, 564. [CrossRef]
42. Wang, L.; Xue, J.; Wang, Q. Correlation between arc mode, microstructure, and mechanical properties during wire arc additive manufacturing of 316L stainless steel. *Mater. Sci. Eng. A* **2019**, *751*, 183–190. [CrossRef]
43. Hosseini, V.; Högström, M.; Hurtig, K.; Valiente Bermejo, M.A.; Stridh, L.E.; Karlsson, L. Wire-arc additive manufacturing of a duplex stainless steel: Thermal cycle analysis and microstructure characterization. *Weld. World* **2019**, *63*, 975–987. [CrossRef]
44. Birmingham, M.; StJohn, D.; Easton, M.; Yuan, L.; Dargusch, M. Revealing the Mechanisms of Grain Nucleation and Formation During Additive Manufacturing. *JOM* **2020**, *72*, 1065–1073. [CrossRef]
45. DebRoy, T.; Wei, H.L.; Zuback, J.S.; Mukherjee, T.; Elmer, J.W.; Milewski, J.O.; Beese, A.M.; Wilson-Heid, A.; De, A.; Zhang, W. Additive manufacturing of metallic components—Process, structure and properties. *Prog. Mater. Sci.* **2018**, *92*, 112–224. [CrossRef]
46. St John, D.H.; McDonald, S.D.; Birmingham, M.J.; Mereddy, S.; Prasad, A.; Dargusch, M. The challenges associated with the formation of equiaxed grains during additive manufacturing of titanium alloys. *Key Eng. Mater.* **2018**, *770*, 155–164. [CrossRef]
47. StJohn, D.H.; Qian, M.; Easton, M.A.; Cao, P. The Interdependence Theory: The relationship between grain formation and nucleant selection. *Acta Mater.* **2011**, *59*, 4907–4921. [CrossRef]
48. Liberini, M.; Astarita, A.; Campatelli, G.; Scippa, A.; Montevicchi, F.; Venturini, G.; Durante, M.; Boccarusso, L.; Minutolo, F.M.C.; Squillace, A. Selection of optimal process parameters for Wire Arc additive manufacturing. *Procedia CIRP* **2017**, *62*, 470–474. [CrossRef]
49. Bontha, S.; Klingbeil, N.W.; Kobryn, P.A.; Fraser, H.L. Effects of process variables and size-scale on solidification microstructure in beam-based fabrication of bulky 3D structures. *Mater. Sci. Eng. A* **2009**, *513–514*, 311–318. [CrossRef]

50. Xu, W.; Lui, E.W.; Pateras, A.; Qian, M.; Brandt, M. In situ tailoring microstructure in additively manufactured Ti-6Al-4V for superior mechanical performance. *Acta Mater.* **2017**, *125*, 390–400. [[CrossRef](#)]
51. Erdakov, I.; Glebov, L.; Pashkeev, K.; Bykov, V.; Bryk, A.; Lezin, V.; Radionova, L. Effect of the Ti6Al4V Alloy Track Trajectories on Mechanical Properties in Direct Metal Deposition. *Machines* **2020**, *8*, 79. [[CrossRef](#)]
52. Kushwaha, A.; Kumar, S.A.; Velu, R. Selective laser melting of titanium alloys: Effect of processing parameters on microstructure and mechanical properties. *Int. J. Mechatron. Manuf. Syst.* **2021**, *14*, 128–142. [[CrossRef](#)]
53. Zhang, Q.; Chen, J.; Lin, X.; Tan, H.; Huang, W.D. Grain morphology control and texture characterization of laser solid formed Ti6Al2Sn2Zr3Mo1.5Cr2Nb titanium alloy. *J. Mater. Process. Technol.* **2016**, *238*, 202–211. [[CrossRef](#)]
54. Rosli, N.A.; Alkahari, M.R.; bin Abdollah, M.F.; Maidin, S.; Ramli, F.R.; Herawan, S.G. Review on effect of heat input for wire arc additive manufacturing process. *J. Mater. Res. Technol.* **2021**, *11*, 2127–2145. [[CrossRef](#)]
55. Kisielawicz, A.; Thalavai Pandian, K.; Sthen, D.; Hagqvist, P.; Valiente Bermejo, M.A.; Sikström, F.; Ancona, A. Hot-Wire Laser-Directed Energy Deposition: Process Characteristics and Benefits of Resistive Pre-Heating of the Feedstock Wire. *Metals* **2021**, *11*, 634. [[CrossRef](#)]
56. Wang, J.; Lin, X.; Wang, J.; Yang, H.; Zhou, Y.; Wang, C.; Li, Q.; Huang, W. Grain morphology evolution and texture characterization of wire and arc additive manufactured Ti-6Al-4V. *J. Alloys Compd.* **2018**, *768*, 97–113. [[CrossRef](#)]
57. Zhuo, Y.; Yang, C.; Fan, C.; Lin, S.; Chen, Y.; Chen, C.; Cai, X. Grain refinement of wire arc additive manufactured titanium alloy by the combined method of boron addition and low frequency pulse arc. *Mater. Sci. Eng. A* **2020**, *805*, 140557. [[CrossRef](#)]
58. Davis, A.E.; Hönnige, J.R.; Martina, F.; Prangnell, P.B. Quantification of strain fields and grain refinement in Ti-6Al-4V inter-pass rolled wire-arc AM by EBSD misorientation analysis. *Mater. Charact.* **2020**, *170*, 110673. [[CrossRef](#)]
59. Hönnige, J.; Colegrove, P.; Prangnell, P.; Ho, A.; Williams, S. The Effect of Thermal History on Microstructural Evolution, Cold-Work Refinement and α/β Growth in Ti-6Al-4V Wire + Arc AM. *arXiv* **2018**, arXiv:1811.02903.
60. Donoghue, J.; Antony, A.A.; Martina, F.; Colegrove, P.A.; Williams, S.W.; Prangnell, P.B. The effectiveness of combining rolling deformation with Wire-Arc Additive Manufacture on β -grain refinement and texture modification in Ti-6Al-4V. *Mater. Charact.* **2016**, *114*, 103–114. [[CrossRef](#)]
61. Ding, D.; Wu, B.; Pan, Z.; Qiu, Z.; Li, H. Wire arc additive manufacturing of Ti6Al4V using active interpass cooling. *Mater. Manuf. Process.* **2020**, *35*, 845–851. [[CrossRef](#)]
62. Brandl, E.; Schoberth, A.; Leyens, C. Morphology, microstructure, and hardness of titanium (Ti-6Al-4V) blocks deposited by wire-feed additive layer manufacturing (ALM). *Mater. Sci. Eng. A* **2012**, *532*, 295–307. [[CrossRef](#)]
63. Artaza, T.; Suárez, A.; Veiga, F.; Braceras, I.; Tabernero, I.; Larrañaga, O.; Lamikiz, A. Wire arc additive manufacturing Ti6Al4V aeronautical parts using plasma arc welding: Analysis of heat-treatment processes in different atmospheres. *J. Mater. Res. Technol.* **2020**, *9*, 15454–15466. [[CrossRef](#)]
64. Martina, F.; Colegrove, P.A.; Williams, S.W.; Meyer, J. Microstructure of Interpass Rolled Wire + Arc Additive Manufacturing Ti-6Al-4V Components. *Metall. Mater. Trans. A* **2015**, *46*, 6103–6118. [[CrossRef](#)]
65. Birmingham, M.J.; McDonald, S.D.; Dargusch, M.S.; StJohn, D.H. Grain-refinement mechanisms in titanium alloys. *J. Mater. Res.* **2008**, *23*, 97–104. [[CrossRef](#)]
66. Wang, F.; Mei, J.; Wu, X. Microstructure study of direct laser fabricated Ti alloys using powder and wire. *Appl. Surf. Sci.* **2006**, *253*, 1424–1430. [[CrossRef](#)]
67. Brandl, E.; Baufeld, B.; Leyens, C.; Gault, R. Additive manufactured Ti-6Al-4V using welding wire: Comparison of laser and arc beam deposition and evaluation with respect to aerospace material specifications. *Phys. Procedia* **2010**, *5*, 595–606. [[CrossRef](#)]
68. Mok, S.H.; Bi, G.; Folkes, J.; Pashby, I.; Segal, J. Deposition of Ti-6Al-4V using a high power diode laser and wire, Part II: Investigation on the mechanical properties. *Surf. Coat. Technol.* **2008**, *202*, 4613–4619. [[CrossRef](#)]
69. Baufeld, B.; Van der Biest, O.; Gault, R. Additive manufacturing of Ti-6Al-4V components by shaped metal deposition: Microstructure and mechanical properties. *Mater. Des.* **2010**, *31*, S106–S111. [[CrossRef](#)]
70. Kurz, W.; Fisher, D.J. *Fundamentals of Solidification*; Trans Tech Publications: Aedermannsdorf, Switzerland, 1989.
71. Ștefănescu, D.M. Equilibrium and non-equilibrium during solidification. In *Science and Engineering of Casting Solidification*, 2nd ed.; Springer: Boston, MA, USA, 2009; pp. 1–20.
72. Fredriksson, H.; Åkerlind, U. Nucleation. In *Solidification and Crystallization Processing in Metals and Alloys*; John Wiley & Sons, Ltd.: Hoboken, NJ, USA, 2012; pp. 166–200.
73. Tedman-Jones, S.N.; McDonald, S.D.; Birmingham, M.J.; StJohn, D.H.; Dargusch, M.S. A new approach to nuclei identification and grain refinement in titanium alloys. *J. Alloys Compd.* **2019**, *794*, 268–284. [[CrossRef](#)]
74. Birmingham, M.J.; Kent, D.; Zhan, H.; StJohn, D.H.; Dargusch, M.S. Controlling the microstructure and properties of wire arc additive manufactured Ti-6Al-4V with trace boron additions. *Acta Mater.* **2015**, *91*, 289–303. [[CrossRef](#)]
75. Birmingham, M.J.; McDonald, S.D.; Dargusch, M.S. Effect of trace lanthanum hexaboride and boron additions on microstructure, tensile properties and anisotropy of Ti-6Al-4V produced by additive manufacturing. *Mater. Sci. Eng. A* **2018**, *719*, 1–11. [[CrossRef](#)]
76. Kennedy, J.R.; Davis, A.E.; Caballero, A.E.; Williams, S.; Pickering, E.J.; Prangnell, P.B. The potential for grain refinement of Wire-Arc Additive Manufactured (WAAM) Ti-6Al-4V by ZrN and TiN inoculation. *Addit. Manuf.* **2021**, *40*, 101928. [[CrossRef](#)]
77. Mereddy, S.; Birmingham, M.J.; Kent, D.; Dehghan-Manshadi, A.; StJohn, D.H.; Dargusch, M.S. Trace carbon addition to refine microstructure and enhance properties of additive-manufactured Ti-6Al-4V. *JOM* **2018**, *70*, 1670–1676. [[CrossRef](#)]

78. Rodrigues, T.A.; Duarte, V.; Miranda, R.M.; Santos, T.G.; Oliveira, J.P. Current Status and Perspectives on Wire and Arc Additive Manufacturing (WAAM). *Materials* **2019**, *12*, 1121. [[CrossRef](#)]
79. Baufeld, B.; Brandl, E.; Van Der Biest, O. Wire based additive layer manufacturing: Comparison of microstructure and mechanical properties of Ti-6Al-4V components fabricated by laser-beam deposition and shaped metal deposition. *J. Mater. Process. Technol.* **2011**, *211*, 1146–1158. [[CrossRef](#)]
80. Colegrove, P.A.; Coules, H.E.; Fairman, J.; Martina, F.; Kashoob, T.; Mamash, H.; Cozzolino, L.D. Microstructure and residual stress improvement in wire and arc additively manufactured parts through high-pressure rolling. *J. Mater. Process. Technol.* **2013**, *213*, 1782–1791. [[CrossRef](#)]
81. Wu, B.; Pan, Z.; Ding, D.; Cuiuri, D.; Li, H.; Fei, Z. The effects of forced interpass cooling on the material properties of wire arc additively manufactured Ti6Al4V alloy. *J. Mater. Process. Technol.* **2018**, *258*, 97–105. [[CrossRef](#)]
82. Li, G.; Qu, S.; Xie, M.X.; Li, X. Effect of ultrasonic surface rolling at low temperatures on surface layer microstructure and properties of HIP Ti-6Al-4V alloy. *Surf. Coat. Technol.* **2017**, *316*, 75–84. [[CrossRef](#)]
83. Xiaogang, J. The Effect of Ultrasonic Vibration on the Solidification of Light Alloys. Ph.D. Thesis, University of Tennessee, Knoxville, TN, USA, 2005.
84. Kumar, S.; Wu, C.S.; Padhy, G.K.; Ding, W. Application of ultrasonic vibrations in welding and metal processing: A status review. *J. Manuf. Process.* **2017**, *26*, 295–322. [[CrossRef](#)]
85. Ning, F.; Hu, Y.; Liu, Z.; Cong, W.; Li, Y.; Wang, X. Ultrasonic Vibration-Assisted Laser Engineered Net Shaping of Inconel 718 Parts: A Feasibility Study. *Procedia Manuf.* **2017**, *10*, 771–778. [[CrossRef](#)]
86. Wang, H.; Hu, Y.; Ning, F.; Cong, W. Ultrasonic vibration-assisted laser engineered net shaping of Inconel 718 parts: Effects of ultrasonic frequency on microstructural and mechanical properties. *J. Mater. Process. Technol.* **2019**, *276*, 116395. [[CrossRef](#)]
87. Todaro, C.J.; Easton, M.A.; Qiu, D.; Zhang, D.; Bermingham, M.J.; Lui, E.W.; Brandt, M.; StJohn, D.H.; Qian, M. Grain structure control during metal 3D printing by high-intensity ultrasound. *Nat. Commun.* **2020**, *11*, 142. [[CrossRef](#)]
88. Criales, L.E.; Arisoy, Y.M.; Lane, B.; Moylan, S.; Donmez, A.; Özel, T. Laser powder bed fusion of nickel alloy 625: Experimental investigations of effects of process parameters on melt pool size and shape with spatter analysis. *Int. J. Mach. Tools Manuf.* **2017**, *121*, 22–36. [[CrossRef](#)]
89. Criales, L.E.; Özel, T. Temperature profile and melt depth in laser powder bed fusion of Ti-6Al-4V titanium alloy. *Prog. Addit. Manuf.* **2017**, *2*, 169–177. [[CrossRef](#)]
90. Criales, L.E.; Arisoy, Y.M.; Lane, B.; Moylan, S.; Donmez, A.; Özel, T. Predictive modeling and optimization of multi-track processing for laser powder bed fusion of nickel alloy 625. *Addit. Manuf.* **2017**, *13*, 14–36. [[CrossRef](#)]
91. Yang, L.; Özel, T. Physics-based simulation models for digital twin development in laser powder bed fusion. *Int. J. Mechatron. Manuf. Syst.* **2021**, *14*, 143–162. [[CrossRef](#)]
92. DebRoy, T.; Mukherjee, T.; Wei, H.L.; Elmer, J.W.; Milewski, J.O. Metallurgy, mechanistic models and machine learning in metal printing. *Nat. Rev. Mater.* **2021**, *6*, 48–68. [[CrossRef](#)]
93. Lee, J.L.; Bhadeshia, H.K.D.H. A methodology for the prediction of time-temperature-transformation diagrams. *Mater. Sci. Eng. A* **1993**, *171*, 223–230. [[CrossRef](#)]
94. Maynier, P.H.; Dollet, J.; Bastien, P. Prediction of Microstructure via Empirical Formulas based on CCT Diagrams. *Metall. Soc. AIME* **1978**, 163–178.
95. Kumar, A.; Mishra, S.; Debroy, T.; Elmer, J.W. Optimization of the Johnson-Mehl-Avrami equation parameters for α -ferrite to γ -austenite transformation in steel welds using a genetic algorithm. *Metall. Mater. Trans. A* **2005**, *36*, 15–22. [[CrossRef](#)]
96. Liu, J.; Jalalahmadi, B.; Guo, Y.B.; Sealy, M.P.; Bolander, N. A review of computational modeling in powder-based additive manufacturing for metallic part qualification. *Rapid Prototyp. J.* **2018**, *24*, 1245–1264. [[CrossRef](#)]
97. Zhang, Z.; Tan, Z.; Yao, X.; Hu, C.; Ge, P.; Wan, Z.; Li, J.; Wu, Q. Numerical methods for microstructural evolutions in laser additive manufacturing. *Comput. Math. Appl.* **2019**, *78*, 2296–2307. [[CrossRef](#)]
98. Zhu, H.; Chen, F.; Zhang, H.; Cui, Z. Review on modeling and simulation of microstructure evolution during dynamic recrystallization using cellular automaton method. *Sci. China Technol. Sci.* **2019**, *63*, 357–396. [[CrossRef](#)]
99. Gatsos, T.; Eslayed, K.A.; Zhai, Y.; Lados, D.A. Review on Computational Modeling of Process–Microstructure–Property Relationships in Metal Additive Manufacturing. *JOM* **2020**, *72*, 403–419. [[CrossRef](#)]
100. Arisoy, Y.M.; Criales, L.E.; Özel, T. Modeling and simulation of thermal field and solidification in laser powder bed fusion of nickel alloy IN625. *Opt. Laser Technol.* **2019**, *109*, 278–292. [[CrossRef](#)]
101. Liu, X.; Li, H.; Zhan, M. A review on the modeling and simulations of solid-state diffusional phase transformations in metals and alloys. *Manuf. Rev.* **2018**, *5*, 10. [[CrossRef](#)]
102. Zinovieva, O.; Zinoviev, A.; Ploshikhin, V. Three-dimensional modeling of the microstructure evolution during metal additive manufacturing. *Comput. Mater. Sci.* **2018**, *141*, 207–220. [[CrossRef](#)]
103. Rodgers, T.M.; Madison, J.D.; Tikare, V. Simulation of metal additive manufacturing microstructures using kinetic Monte Carlo. *Comput. Mater. Sci.* **2017**, *135*, 78–89. [[CrossRef](#)]
104. Lian, Y.; Gan, Z.; Yu, C.; Kats, D.; Liu, W.K.; Wagner, G.J. A cellular automaton finite volume method for microstructure evolution during additive manufacturing. *Mater. Des.* **2019**, *169*, 107672. [[CrossRef](#)]
105. Benakis, M.; Costanzo, D.; Patran, A. Current mode effects on weld bead geometry and heat affected zone in pulsed wire arc additive manufacturing of Ti-6-4 and Inconel 718. *J. Manuf. Process.* **2020**, *60*, 61–74. [[CrossRef](#)]

106. Wan, H.; Chen, G.; Li, C.; Qi, X.; Zhang, G. Data-Driven evaluation of fatigue performance of additive manufactured parts using miniature specimens. *J. Mater. Sci. Technol.* **2019**, *35*, 1137–1146. [[CrossRef](#)]
107. Popova, E.; Rodgers, T.M.; Gong, X.; Cecen, A.; Madison, J.D.; Kalidindi, S.R. Process-Structure linkages using a data science approach: Application to simulated additive manufacturing data. *Integr. Mater. Manuf. Innov.* **2017**, *6*, 54–68. [[CrossRef](#)]
108. Wohlers, T. *Wohlers Report 2021: 3D Printing and Additive Manufacturing State of the Industry*; Annual Worldwide Progress Report; Wohlers Associates: Fort Collins, CO, USA, 2021.

Disclaimer/Publisher’s Note: The statements, opinions and data contained in all publications are solely those of the individual author(s) and contributor(s) and not of MDPI and/or the editor(s). MDPI and/or the editor(s) disclaim responsibility for any injury to people or property resulting from any ideas, methods, instructions or products referred to in the content.